J Electr Eng Technol.2018; 13(4): 1603-1612
http://doi.org/10.5370/JEET.2018.13.4.1603

ISSN(Print) 1975-0102
ISSN(Online) 2093-7423

Small-Size Induction Machine Equivalent Circuit Including Variable Stray Load and Iron Losses

Mateo Bašić† and Dinko Vukadinović*

Abstract – The paper presents the equivalent circuit of an induction machine (IM) model which includes fundamental stray load and iron losses. The corresponding equivalent resistances are introduced and modeled as variable with respect to the stator frequency and flux. Their computation does not require any tests apart from those imposed by international standards, nor does it involve IM constructional details. In addition, by the convenient positioning of these resistances within the proposed equivalent circuit, the order of the conventional IM model is preserved, thus restraining the inevitable increase of the computational complexity. In this way, a compromise is achieved between the complexity of the analyzed phenomena on the one hand and the model's practicability on the other. The proposed model has been experimentally verified using four IMs of different efficiency class and rotor cage material, all rated 1.5 kW. Besides enabling a quantitative insight into the impact of the stray load and iron losses on the operation of mains-supplied and vector-controlled IMs, the proposed model offers an opportunity to develop advanced vector control algorithms since vector control is based on the fundamental harmonic component of IM variables.

Keywords: Equivalent circuit, Induction machine, Iron losses, Modeling, Stray load losses

1. Introduction

The iron losses are commonly considered 1% - 4% of the induction machine (IM) rated power, whereas the stray load losses (SLLs) are considered 0.5% - 3% of the IM rated power at full load [1]. These percentages, it may be argued, are not negligible. Besides, a recent study has shown that these percentages may be well underestimated for small IMs, particularly those with low efficiency [2]. In addition, adverse effects of ignoring these losses in IM vector control algorithms were reported in [3-5]. By adding to this the reduction of the IM's efficiency and loading capacity, and the increase in the IM's operating temperature, all as a result of these losses, the importance of their assessment in small IMs becomes critical.

The IM iron losses vary with respect to the frequency and the magnetic flux density of the applied magnetic field. They are traditionally divided into the hysteresis component (proportional to the frequency) and the eddy-current component (proportional to the square of the frequency), whereas in some cases, the excess-loss component is further separated from the classical eddy-current component [6]. Compared to the iron losses, the theoretical background of the SLLs is more complex. An overview and a discussion of their many origins are provided in [7]. In a nutshell, they occur in IMs due to theoretical and manufacturing imperfections, and are seen as the sum total of loss components not encompassed by the conventional losses. The iron losses and, to a lesser degree, the SLLs can be determined with reasonable accuracy from tests imposed by the international standards IEEE 112-B [8] and IEC 60034-2-1 [9]. Yet, these standards only consider the stator voltage amplitude and the load torque as the causes of variation of the iron losses and the SLLs, respectively, while disregarding other factors.

In IM equivalent circuits, the iron losses are standardly represented by the equivalent resistance, R_m, placed in parallel with the magnetizing inductance, L_m [3, 4, 10-12]. Such configuration, however, increases the order of the IM model compared to the conventional model, which makes it computationally more demanding. A configuration in which R_m is placed in the transverse branch right to the stator resistance was proposed in [13]. It was later considered in [5, 14-17], where its effectiveness was proven experimentally both for IM analysis and control. The configuration proposed in [13] ensures the accuracy comparable to the standard iron-loss configuration, but without increasing the order of the IM model. In addition, R_m is, for convenience, most often modeled as a constant parameter, as in [11, 12, 17]. A more meaningful effort to model the iron-loss resistance as linearly dependent on the supply frequency is reported in [3, 4]. But arguably the most complete iron-loss representation is found in [14], where R_m was taken as variable with respect to both the stator frequency and the magnitude of the stator flux-linkage vector (in the following: *stator flux*). However, the proposed R_m identification scheme implies elaborate and

† Corresponding Author: Faculty of Electrical Engineering, Mechanical Engineering and Naval Architecture, University of Split, Croatia. (mabasic@fesb.hr)
* Faculty of Electrical Engineering, Mechanical Engineering and Naval Architecture, University of Split, Croatia. (dvukad@fesb.hr)
Received: January 18, 2018; Accepted: March 14, 2018

Copyright ⓒ The Korean Institute of Electrical Engineers
This is an Open-Access article distributed under the terms of the Creative Commons Attribution Non-Commercial License (http://creativecommons.org/licenses/by-nc/3.0/) which permits unrestricted non-commercial use, distribution, and reproduction in any medium, provided the original work is properly cited.

time consuming testing and data processing.

Very few papers consider the SLL equivalent resistances as part of the IM equivalent circuit, usually placed in parallel with the stator and/or rotor leakage inductances to take into account losses associated with the leakage fluxes [3, 18, 19]. A different SLL configuration that does not increase the order of the IM model was proposed in [7], where the SLL resistance is connected in series with the stator phase resistance. This configuration was later considered in several other papers [10-12, 17, 18], where its validity was proven experimentally on different-size IMs. All the models in literature that attempt to represent the SLLs include the iron losses as well. Within these models, the SLL resistance is taken either as a constant parameter [12, 17], or as variable with respect to the stator frequency [3, 10, 19], or as variable with respect to the stator voltage amplitude (i.e., stator flux) [11]. However, to our best knowledge, the SLL resistance, R_{add}, has not yet been considered as variable with respect to both stator frequency and flux.

In this paper, a hybrid configuration with respect to those proposed in [7] and [13] is considered for modeling of the IM iron losses and SLLs. Such configuration was already adopted in [17], but, unlike there, here both R_m and R_{add} are modeled as variable with respect to the stator frequency and flux. Simple estimation formulas for R_m and R_{add} are derived from extensive test data. It should be underlined, however, that the proposed model is valid only for a fundamental harmonic of the supply.

2. Proposed Induction Machine Model

Fig. 1 shows the equivalent circuit of the proposed IM model in the stationary reference frame. Note that only the circuit for the α-axis is given since all the physical phenomena along the β-axis are analogous (with a phase shift of 90° el.).

In Fig. 1, R_s and R_r denote the stator and rotor phase resistance, respectively; u_s denotes the stator voltage, whereas i_s and i_r denote the stator and rotor current, respectively; i_{Rm}, i_m, and i_L denote the iron-loss current, the magnetizing current, and the stator inductance current, respectively; $L_{\sigma s}$ and $L_{\sigma r}$ denote the stator and rotor leakage inductance, respectively; ψ_s and ψ_r denote the stator and rotor flux linkage, respectively; ω_r denotes the rotor angular speed in electrical rad/s.

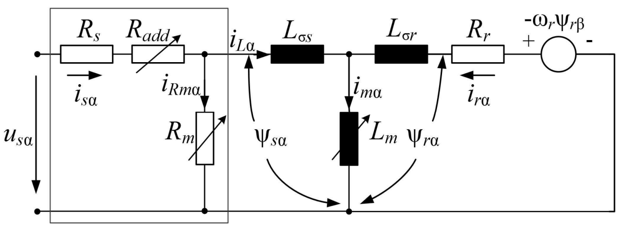

Fig. 1. Equivalent circuit of the proposed IM model in the stationary reference frame (α-axis)

Note that by placing R_{add} in series with R_s, as in the proposed model, it is implied that the SLL resistance takes a share of the no-load losses as well. This means that the conventional iron losses, as determined from the standard no-load test, have to be split into the actual iron losses and additional no-load losses, as discussed in [12]. Consequently, a correction of the R_m value determined from the standard no-load test is required, as discussed in Section 3.

Next, the Thevenin equivalents are introduced for the elements in the rectangle in Fig. 1, so the equivalent circuit in Fig. 2 is obtained. The differential equations describing the proposed IM model are thus given as follows:

$$u_{sT\alpha} = R_{sT} i_{sT\alpha} + \frac{d\psi_{s\alpha}}{dt}, \; u_{sT\beta} = R_{sT} i_{sT\beta} + \frac{d\psi_{s\beta}}{dt} \tag{1}$$

$$0 = R_r i_{r\alpha} + \frac{d\psi_{r\alpha}}{dt} + \omega_r \psi_{r\beta}, \; 0 = R_r i_{r\beta} + \frac{d\psi_{r\beta}}{dt} - \omega_r \psi_{r\alpha} \tag{2}$$

$$\psi_{s\alpha} = L_{\sigma s} i_{sT\alpha} + L_m i_{m\alpha}, \; \psi_{s\beta} = L_{\sigma s} i_{sT\beta} + L_m i_{m\beta} \tag{3}$$

$$\psi_{r\alpha} = L_{\sigma r} i_{r\alpha} + L_m i_{m\alpha}, \; \psi_{r\beta} = L_{\sigma r} i_{r\beta} + L_m i_{m\beta} \tag{4}$$

$$i_{m\alpha} = i_{sT\alpha} + i_{r\alpha}, \; i_{m\beta} = i_{sT\beta} + i_{r\beta} \tag{5}$$

$$T_e = \frac{3}{2} p \frac{L_m}{L_r} (\psi_{r\alpha} i_{sT\beta} - \psi_{r\beta} i_{sT\alpha}) = T_L + J\frac{d\omega_r}{dt} + B\omega_r \tag{6}$$

where T_e is the induced electromagnetic torque, L_r is the rotor inductance, p is the number of pole pairs, T_L is the load torque, J is the moment of inertia, and B is the rotational friction coefficient.

The Thevenin equivalents in (1)-(6) are denoted by T in the subscript and are calculated as

$$R_{sT} = \frac{(R_s + R_{add})R_m}{R_s + R_{add} + R_m} \tag{7}$$

$$u_{sT\alpha} = u_{s\alpha} \frac{R_m}{R_s + R_{add} + R_m}, \; u_{sT\beta} = u_{s\beta} \frac{R_m}{R_s + R_{add} + R_m} \tag{8}$$

$$i_{sT\alpha} = i_{s\alpha} \frac{R_s + R_{add} + R_m}{R_m} - \frac{u_{s\alpha}}{R_m}, \; i_{sT\beta} = i_{s\beta} \frac{R_s + R_{add} + R_m}{R_m} - \frac{u_{s\beta}}{R_m} \tag{9}$$

Note that the configuration of the equivalent circuit in Fig. 2 is the same as that of the well-known conventional

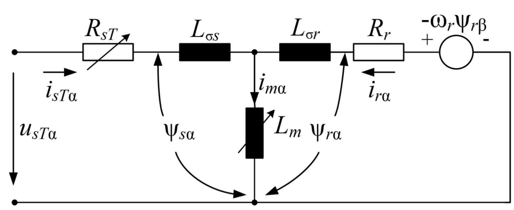

Fig. 2. Simplified equivalent circuit of the proposed IM model in the stationary reference frame (α-axis)

IM model, whereas the only difference between (1)-(6) and the corresponding equations of the conventional model is in the used notation. Therefore, the introduction of R_m and R_{add} in the proposed manner does not increase the number of differential equations with which the IM model is described (i.e., the model's order) compared to the conventional IM model, which reflects the computational elegance of the proposed model.

3. Determination of the Equivalent Circuit Parameters

The resistance R_s was determined from the standard dc-supply test, with the average value of all three phases taken as final and corrected to 25 °C. The resistance R_r was determined by Method 4 from [8] – modified to include R_{add} in the respective equations – and subsequently corrected to 25 °C. A classical locked-rotor test is not recommended in this case since it requires accurate knowledge of the R_{add} value under unity slip. The magnetizing inductance as a function of the magnetizing current magnitude, I_m, was derived from test data recorded during the standard no-load test. In the saturated region, the measurement points obtained for each of the analyzed IMs were approximated by a corresponding curve, whereas in the unsaturated region, L_m was considered constant, as described in [17]. The total leakage inductance was determined from a locked-rotor impedance test at rated frequency and at reduced voltage resulting in approximately rated stator current. Subsequently, it was evenly distributed between the stator and rotor parts of the IM equivalent circuit ($L_{\sigma s} = L_{\sigma r}$). Note that this does not require knowledge of the R_{add} value. The skin effect was not taken into account due to the fact that it may be considered negligible in small IMs).

The testing procedures and the experimental setup for determination of the SLLs and the iron losses are explained in detail in [2]. These procedures involve modifications of the methods imposed by the standards [8] and [9], all aimed at improving the overall accuracy and widening the scope of application (e.g., extending standard no-load and variable-load tests to different supply frequencies). A total of four squirrel-cage IMs (4-pole, star-connected, rated 1.5 kW) were selected for testing: three die-cast aluminum rotor IMs of different efficiency class – IE1, IE2 and IE3 according to IEC 60034-30-1 [20] (in the following: *IM-1*, *IM-2*, and *IM-3*, respectively) – and one die-cast copper rotor IM (in the following: *IM-4*).

3.1 Determination of the SLL equivalent resistance

The SLL resistance is first derived from the measurement data obtained from standard no-load and variable-load tests. The detailed theoretical analysis is provided in [12], so only the final expression is given here as

$$R_{add} = \frac{(P_e - 3R_s I_s^2 - P_{Fe,conv})(1-s) - P_m - P_{loss,mech}}{3(I_s^2 - (1-s)I_{s,0}^2)} \qquad (10)$$

where P_e is the electrical input power, $I_{s,0}$ is the RMS value of the stator current from no-load test, I_s is the RMS value of the stator current, s is the slip, P_m is the mechanical output power on the motor shaft, $P_{loss,mech}$ denotes the friction and windage losses, and $P_{Fe,conv}$ denotes the conventional iron losses, as defined by the international standards [8, 9].

The numerator in (10) represents the corrected SLLs, whereas the denominator represents the squared equivalent SLL current. In this view, it has to be noted that the P_m value in (10) is corrected so the SLLs are equal to zero at zero load torque, as imposed by IEEE 112-B. Similarly, the $P_{Fe,conv}$ value in (10) takes into account the variation of iron losses with load, as imposed by IEC 60034-2-1. Both these corrections have been made to accomplish greater accuracy.

The SLL resistance can be identified as the slope of the regression line of the SLLs vs. squared equivalent SLL current [12]. Fig. 3 shows the regression lines obtained for the four tested IMs. To check the measurement consistency, the variable-load tests were repeated three times for each IM.

During these tests, the measurement of both the ambient temperature (by thermometer) and the stator winding temperature (by thermocouple) was carried out and taken into account for subsequent correction of the IM parameters, as imposed by the international standards.

As it can be seen in Fig. 3, only minor discrepancies were noted between the subsequent variable-load tests. Consequently, the resulting regression lines are, in fact, obtained as linear approximations of the combined measured values. The following R_{add} values were obtained by the described procedure: 2.7739 Ω (IM-1), 1.2320 Ω (IM-2), 1.5198 Ω (IM-3), and 2.7279 Ω (IM-4). These values can be considered valid for all load torques, so the SLL resistance is further on considered as a torque independent parameter. Besides, such determined R_{add} values may as well be declared rated ($R_{add,rated}$) since they are obtained for the rated supply frequency and, additionally, the stator flux variations during these tests were within ±10% of its rated value.

The SLLs as a function of the supply frequency, f_s, were

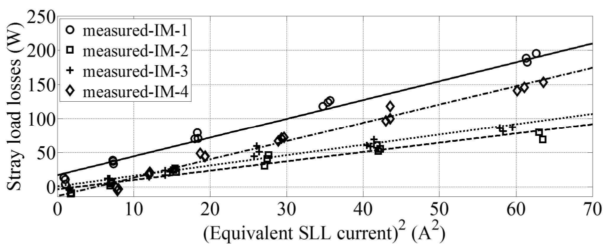

Fig. 3. Regression lines of the SLLs vs. squared equivalent SLL current obtained for the tested IMs at 50 Hz

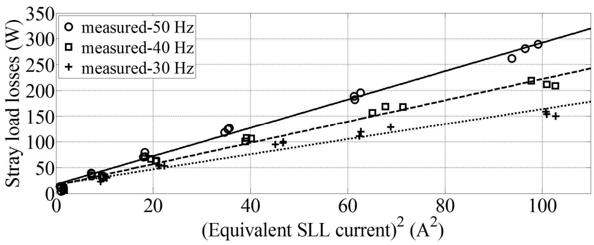

Fig. 4. Regression lines of the SLLs vs. squared equivalent SLL current obtained at different supply frequencies (IM-1)

derived from no-load and variable-load tests performed at three supply frequencies – 30 Hz, 40 Hz, and 50 Hz – by utilizing the open-loop V/f control strategy, as described in [2]. Fig. 4 shows the regression lines of the SLL vs. squared equivalent SLL current obtained for the IM-1.

The slope of the lines in Fig. 4 changes nearly linearly with the supply frequency and similar results were obtained for other tested IMs as well. The R_{add} values obtained from the regression lines' slopes for all the considered supply frequencies and tested IMs are given in Table 1.

The values in the brackets in Table 1 represent the absolute errors between these R_{add} values and those obtained by linear scaling of $R_{add,rated}$ with respect to the supply frequency, i.e.

$$R_{add}(f_s) = R_{add,rated}\frac{f_s}{f_{s,rated}} \tag{11}$$

It can be observed that generally good agreement is achieved between these values. The greatest errors at frequencies lower than the rated are recorded for the IM-3. However, this IM has a rather small R_{add} value already at f_s = 50 Hz and since the SLLs, along with their impact, drop fairly significantly with the supply frequency [2, 10], the observed errors are not expected to have significant impact on the overall accuracy. Hence, the linear scaling of $R_{add,rated}$ as in (11) is in this paper proposed to obtain the R_{add} value at frequencies different from the rated.

The SLLs as a function of the stator flux, Ψ_s, were determined by changing the amplitude of the supply voltage at f_s = 50 Hz and with constant load torque (in the following: *variable-flux test*), as described in [2]. Once the SLLs are identified for different flux values, the corresponding R_{add} values can be obtained from (10). Fig. 5 shows such obtained R_{add} values (denoted *measured*) plotted vs. the stator flux for all the tested IMs.

The measured R_{add} values seem to linearly increase with the stator flux. Therefore, a linear approximation function is applied and corrected by shifting it along the y-axis so that $R_{add} = R_{add,rated}$ is obtained for the rated stator flux. For the IM-1, IM-2, and IM-3, the slope of the regression line is close to the respective $R_{add,rated}$ value, whereas the corresponding y-intercept value is close to zero. Hence, the

Table 1. SLL resistance values for different supply frequencies

	f_s = 50 Hz	f_s = 40 Hz	f_s = 30 Hz
IM-1	2.7739 Ω	2.1006 Ω (+0.1185 Ω)	1.5241 Ω (+0.1402 Ω)
IM-2	1.2320 Ω	0.9579 Ω (+0.0277 Ω)	0.4641 Ω (+0.2751 Ω)
IM-3	1.5198 Ω	0.8710 Ω (+0.3448 Ω)	0.5088 Ω (+0.4031 Ω)
IM-4	2.7279 Ω	2.2172 Ω (–0.0349 Ω)	1.5230 Ω (+0.1137 Ω)

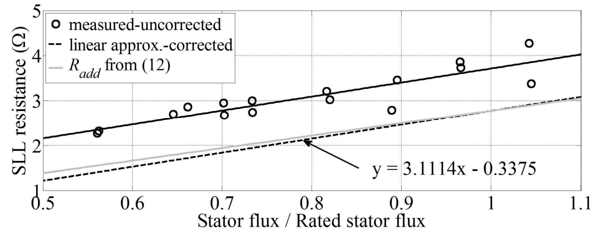

(a)

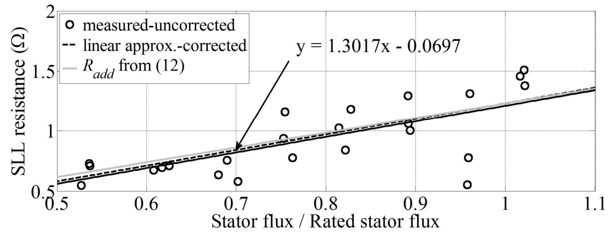

(b)

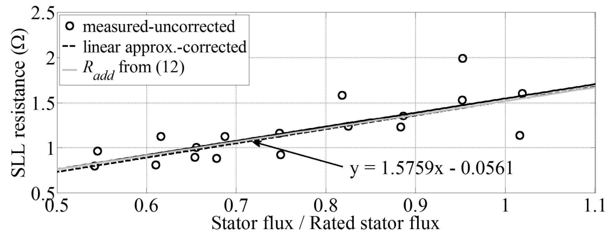

(c)

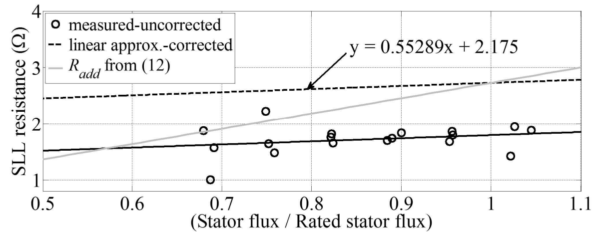

(d)

Fig. 5. Regression lines of R_{add} vs. stator flux obtained for the tested IMs: (a) IM-1, (b) IM-2, (c) IM-3, and (d) IM-4

R_{add}'s dependency on the stator flux may be expressed as

$$R_{add}(\Psi_s) = R_{add,rated}\frac{\Psi_s}{\Psi_{s,rated}} \tag{12}$$

Interestingly, the only exception from this is the IM-4. It is speculated that this may be related with the different rotor material causing maybe somewhat different distribution of the SLLs within the machine. However, for the sake of simplicity and generality, (12) is adopted for this IM as well.

Finally, by combining (11) and (12) into a single expression, the following formula for the assessment of the SLL resistance is obtained:

$$R_{add}(f_s,\Psi_s)=R_{add,rated}\frac{f_s}{f_{s,rated}}\frac{\Psi_s}{\Psi_{s,rated}} \tag{13}$$

Thereby, (13) defines the SLL resistance as both stator frequency and flux dependent parameter – $R_{add}(f_s, \Psi_s)$.

3.2 Determination of the Iron-Loss equivalent resistance

The conventional iron losses were derived from the standard no-load test, only extended to five different supply frequencies in the range 10 Hz - 50 Hz. Subsequently, these losses had to be corrected in order to take into account the existence of the SLL resistance in no-load operation. The correction was done as in [12], [17], but with a difference that R_{add}'s variation with frequency and flux was here also taken into account. The actual iron losses were, thus, calculated as

$$P_{Fe}=P_{Fe,conv}-3I_{s,0}^2\frac{R_{s,no-load}}{R_{s,load}}R_{add}(f_s,\Psi_s) \tag{14}$$

where $R_{s,no-load}$ is the stator phase resistance value during the no-load test and $R_{s,load}$ is the stator phase resistance value in the rated-load thermal conditions, whereas their ratio provides a quick temperature correction of the SLL resistance.

Once the actual iron losses are known for each measurement point, the corresponding R_m values can be calculated from the measurement data, as explained in [14]. However, identification of the iron-loss resistance in such a way requires extensive measurement and computation. So, an alternative approach is here proposed that relies on the assumption of the hysteresis loss dominance in the considered frequency range [2]. Namely, in [2, 21, 22], it was shown that the hysteresis iron losses are dominant within the range $fs \leq 50$ Hz, especially for the IMs of higher efficiency class. Therefore, in order to simplify the analysis, the eddy-current loss component may be neglected in the IM iron loss model at least up to the rated speed.

The fundamental component of the IM's iron losses can be expressed as a function of the stator flux and stator frequency as follows:

$$P_{Fe}=P_{Fe\_h}+P_{Fe\_e}=K_h f_s\Psi_s^2+K_e f_s^2\Psi_s^2 \tag{15}$$

where P_{Fe_h} and P_{Fe_e} are the hysteresis and eddy-current iron losses, respectively, whereas K_h and K_e are the coefficients related to the hysteresis and eddy-current iron losses, respectively.

The coefficients K_h and K_e are commonly considered constant, though there are studies which point to their variation with both the frequency and flux density of the applied magnetic field [23-26]. Still, the dependency of K_h and K_e on the stator frequency may be considered negligible for sinusoidal magnetic fields of frequencies up to 400 Hz and flux densities up to 2 T [23-25], leaving K_h and K_e solely dependent on Ψ_s, i.e., $K_h(\Psi_s)$ and $K_e(\Psi_s)$.

From Fig. 1, the iron losses may also be defined as

$$P_{Fe}=3\frac{E_s^2}{R_m} \tag{16}$$

where E_s is the RMS value of the stator induced electromotive force.

The steady-state amplitude of a sinusoidal stator flux may further be defined as

$$\Psi_s=\frac{\sqrt{2}E_s}{2\pi f_s} \tag{17}$$

Consequently, by combining (15)-(17) and assuming the dependence $K_h(\Psi_s)$ and $K_e(\Psi_s)$, the following is obtained:

$$\frac{K_h(\Psi_s)}{f_s}+K_e(\Psi_s)=\frac{6\pi^2}{R_m} \tag{18}$$

Neglecting the first term on the left side of (18) - related to the hysteresis losses - leaves the iron-loss resistance dependent on the stator flux - through $K_e(\Psi_s)$ - as follows:

$$R_m(\Psi_s)=\frac{6\pi^2}{K_e(\Psi_s)} \tag{19}$$

Conversely, neglecting the second term on the left side of (18) - related to the eddy-current losses - leaves the iron-loss resistance dependent on both the stator frequency and the stator flux - through $K_h(\Psi_s)$ - as follows:

$$R_m(f_s,\Psi_s)=\frac{6\pi^2 f_s}{K_h(\Psi_s)}=K_{h1}(\Psi_s)\cdot f_s \tag{20}$$

With regard to the previous discussion about the dominance of the hysteresis losses in the considered operating range, in this paper, the iron-loss resistance is defined as in (20), i.e., as both stator frequency and flux dependent parameter – $R_m(f_s, \Psi_s)$.

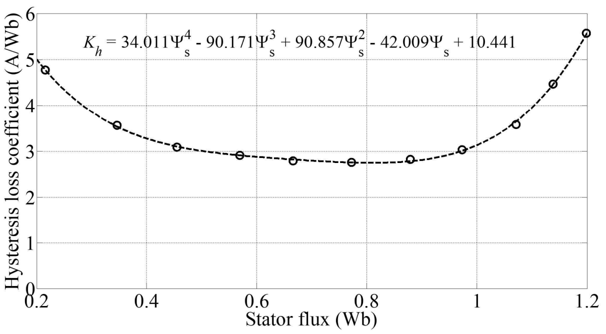

Fig. 6. Hysteresis loss coefficient vs. stator flux (IM-1)

The coefficient $K_h(\Psi_s)$ in (20) is calculated from (15) for each value of P_{Fe} and Ψ_s obtained from the standard no-load test at 50 Hz, by assuming $P_{Fe\_e} = 0$ [2]. Thus obtained values of K_h are then plotted against Ψ_s and interpolated by a polynomial. Fig. 6 shows the variation of K_h with the stator flux for the IM-1, along with the 4th order polynomial fit.

The coefficient $K_{h1}(\Psi_s)$ in (20) is subsequently obtained as $K_{h1}(\Psi_s) = 6\pi^2/K_h(\Psi_s)$, thereby inheriting the stator flux dependency of $K_h(\Psi_s)$.

4. Experimental Validation

In order to determine how well the proposed IM model describes the actual machine, particularly in comparison with the conventional model, two simulation models were built in the MATLAB-Simulink: the proposed model – by using (1)-(9), (13), and (17), and with other parameters determined as described in Section 3 – and the conventional model – with omitted SLLs and iron losses, and with R_r identified from a classical locked-rotor test. Note, however, that by applying a locked-rotor test, a portion of the SLLs is inevitably assigned to the rotor winding losses. In the considered case, this resulted in 20% - 50% greater R_r values compared to Method 4 from [8]. Hence, it may be argued that in this way a portion of the SLLs is taken into account, though unintentionally, even in the conventional IM model - on the rotor side.

Although the conventional model may seem inadequate for comparison, being too easy a target, it was in the end chosen for two reasons: to determine whether its upgrade is really necessary and due to the shear multiplicity of other candidate models (e.g., models with omitted SLLs or iron losses, with differently positioned R_m or R_{add}, with constant R_m or R_{add}, with differently determined R_r, and so on). In any case, the proposed model is ultimately validated by a comparison with the experimental results.

Figs. 7-9 and Figs. 10-12 show the results obtained from variable-load tests at f_s = 50 Hz and f_s = 30 Hz, respectively, whereas Figs. 13 and 14 show the distribution of IM loss components as obtained from variable-load and variable-flux tests, respectively, both at f_s = 50 Hz (IM-2 is left out from the further analysis).

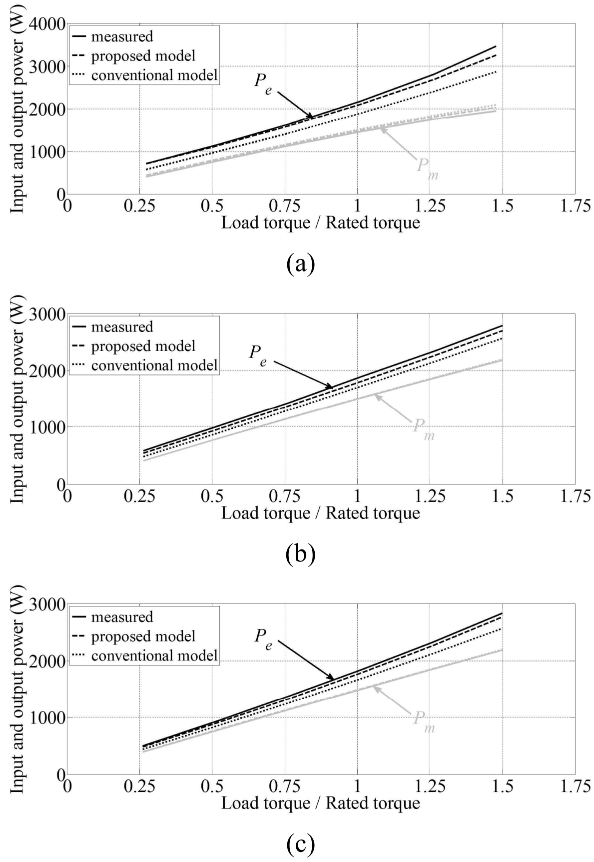

Fig. 7. Electrical input power (P_e) and mechanical output power (P_m) from variable-load tests (f_s = 50 Hz): (a) IM-1, (b) IM-3, and (c) IM-4

In Fig. 7, the input power values obtained from the proposed model are in much better agreement with the measured results as compared to those obtained from the conventional model. The difference between the measured P_e and that obtained by the conventional model notably increases with the load torque, which is mostly due to the SLLs. On the other hand, both models are able to assess the mechanical output power with remarkable accuracy.

Since the load torque is an input parameter in simulations and is set equal to the measured value, the observed differences in P_m between the simulations and experiments – as well as between the two simulation models – are only due to the respective differences in the rotor speed (i.e., slip).

The errors in slip in Fig. 8 are not that substantial for load torques up to the rated, regardless of the IM model. This is especially true for the premium-efficiency machines: IM-3 and IM-4. Still, the errors are notably lower in the case of the proposed model. Similar observations apply in the case of the stator current errors. It is observed that the proposed model provides more accurate account of the stator current than the conventional model at high load torques (i.e., at high SLLs).

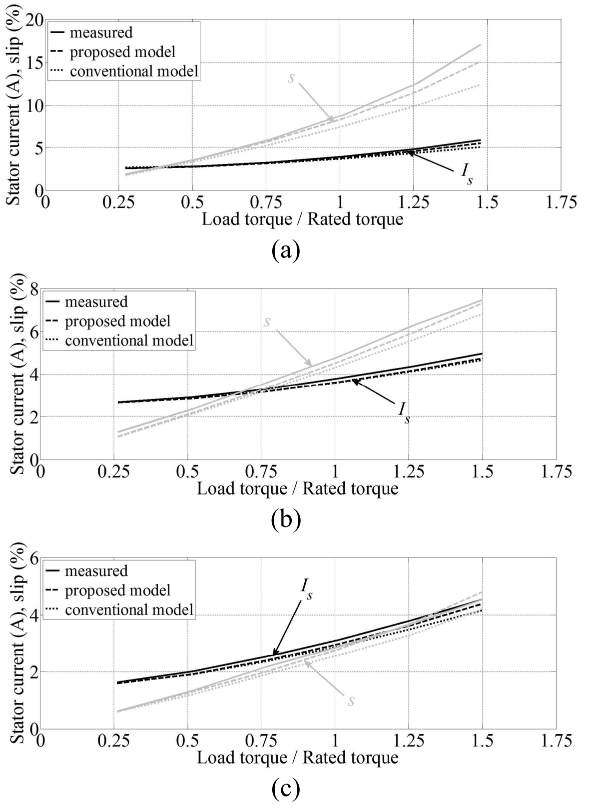

Fig. 8. Stator current (I_s) and slip (s) from variable-load tests (f_s = 50 Hz): (a) IM-1, (b) IM-3, and (c) IM-4

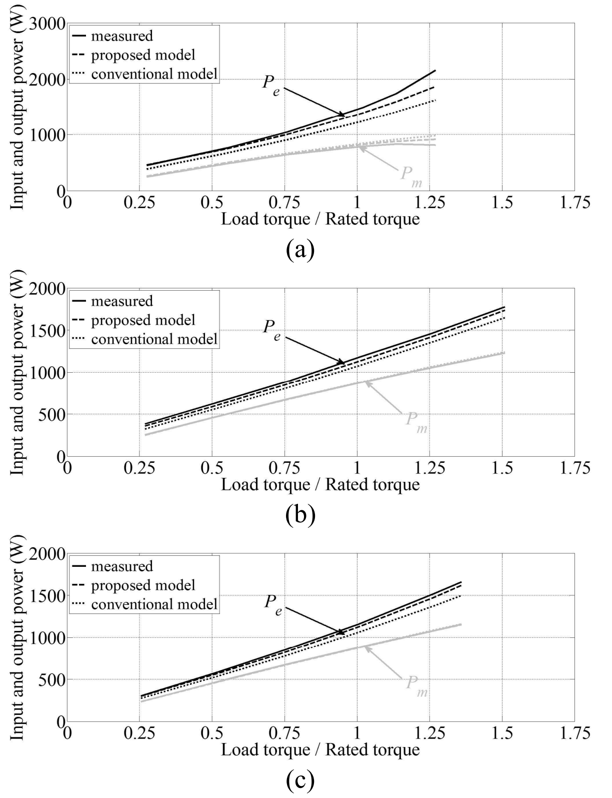

Fig. 10. Electrical input power (P_e) and mechanical output power (P_m) from variable-load tests (f_s = 30 Hz): (a) IM-1, (b) IM-3, and (c) IM-4

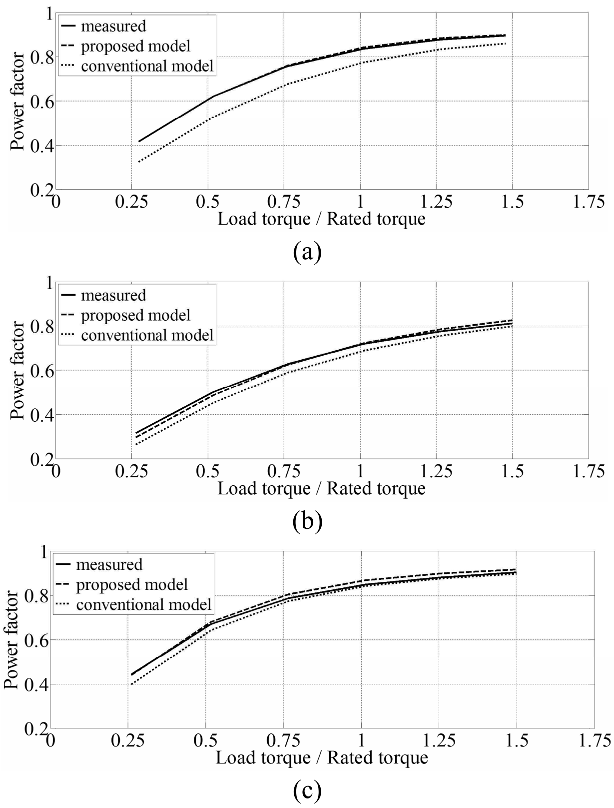

Fig. 9. Power factor from variable-load tests (f_s = 50 Hz): (a) IM-1, (b) IM-3, and (c) IM-4

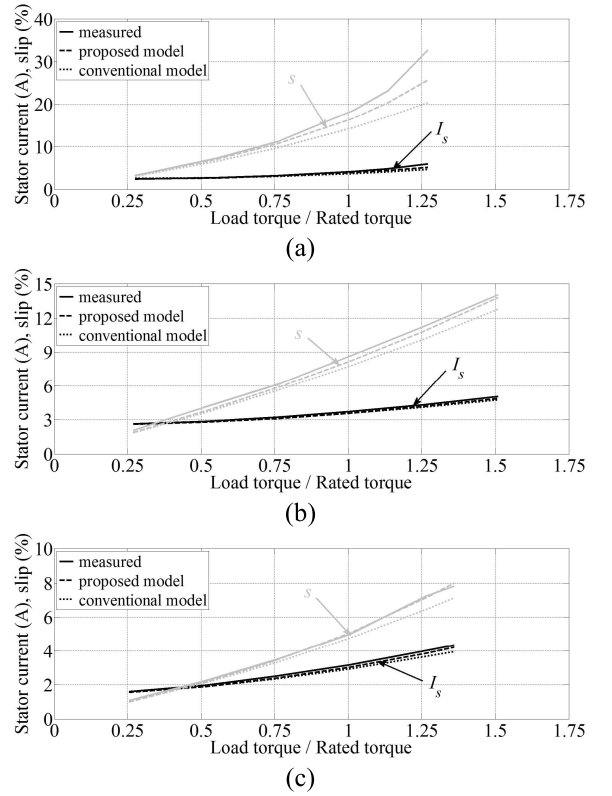

Fig. 11. Stator current (I_s) and slip (s) from variable-load tests (f_s = 30 Hz): (a) IM-1, (b) IM-3, and (c) IM-4

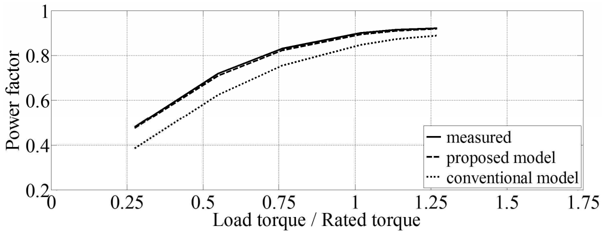

(a)

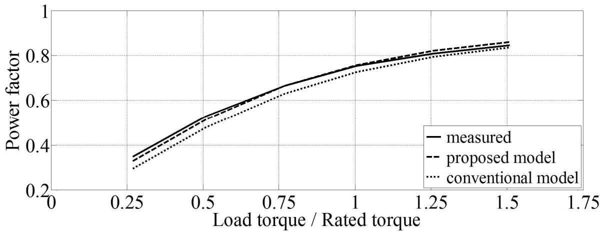

(b)

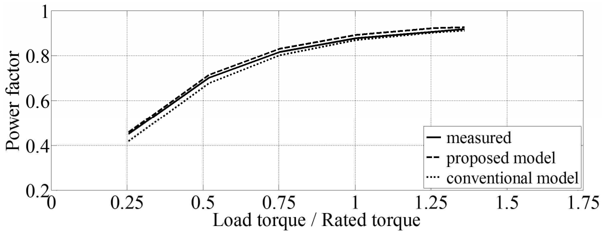

(c)

Fig. 12. Power factor from variable-load tests (f_s = 30 Hz): (a) IM-1, (b) IM-3, and (c) IM-4

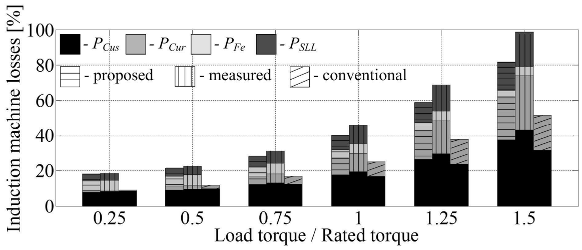

(a)

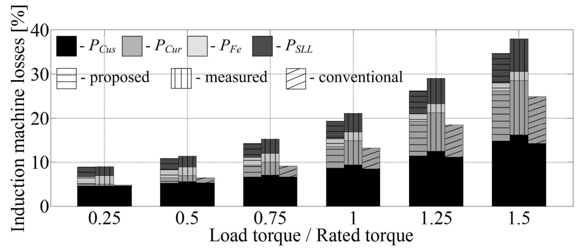

(b)

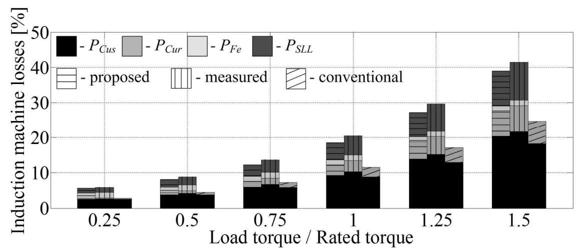

(c)

Fig. 13. IM losses from variable-load tests (stator winding - P_{Cus}, rotor winding - P_{Cur}, iron - P_{Fe}, stray load - P_{SLL}): (a) IM-1, (b) IM-3, and (c) IM-4

Also, quite remarkable is the accuracy with which the power factor is assessed by the proposed model, as seen in Fig. 9, which affirms that the proposed model accurately describes the active and reactive power distribution in the actual machine, as opposed to the conventional model.

The results shown in Figs. 10-12 confirm the superiority of the proposed model even at the supply frequency lower than the rated. As previously anticipated, the errors in the estimated R_{add} values noted for f_s = 30 Hz in Table 1 do not have much impact on the overall accuracy of the proposed IM model.

In Figs. 13 and 14, the IM loss values obtained from variable-load and variable-flux tests are given by components as a percentage of the IM rated power (1.5 kW). Note that the friction and windage losses are omitted from these figures since they are virtually constant for constant supply frequency (for the tested IMs, they amounted to only 1.5% - 3% of the rated power).

As expected, all the loss components in Fig. 13, except for the iron losses, increase with an increase in load. The iron losses decrease slightly with load due to the stator flux reduction. Furthermore, it is evident that the conventional model is inherently unable to accurately evaluate the actual losses. On the other hand, the proposed model provides quite accurate evaluation of the actual losses – both total and by components – and significantly reduces the error introduced by the conventional model. The accuracy of the proposed model slightly drops with an increase in load, which may be due to the approximations built into (13) and (17).

In Fig. 14, both the values and trends of the actual loss components are again followed remarkably well by the proposed model. In this case, the error slightly increases with decreasing flux, which is again probably due to the adopted approximations. On the other hand, the conventional model again fails to provide a satisfactory account of the actual IM losses.

5. Conclusion

In this paper, an IM equivalent circuit is proposed that is able to accurately model the fundamental iron losses and SLLs under various operating conditions. The respective equivalent resistances are taken as dependent on both the stator frequency and flux. Simple formulas are proposed for their calculation and the model is verified

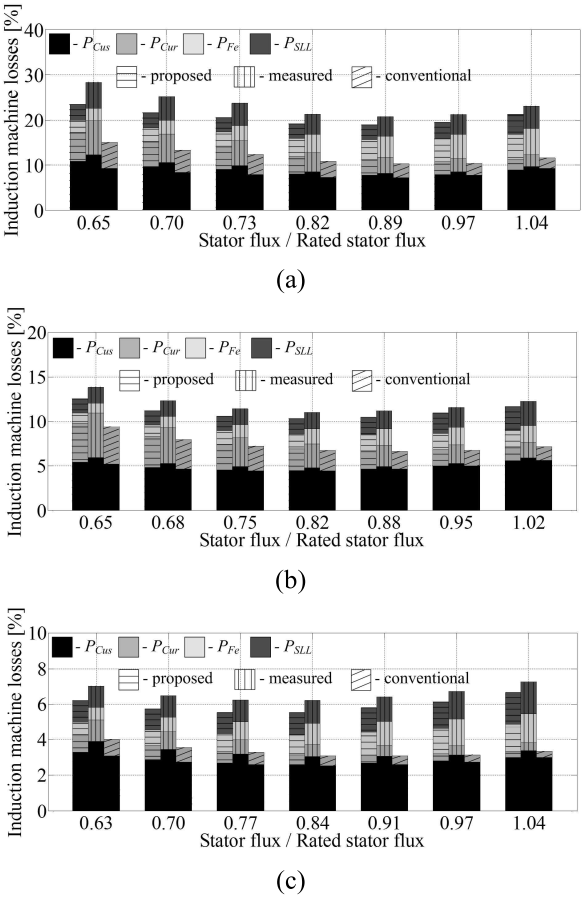

Fig. 14. IM losses from variable-flux tests (stator winding - P_{Cus}, rotor winding - P_{Cur}, iron - P_{Fe}, stray load - P_{SLL}): (a) IM-1, (b) IM-3, and (c) IM-4

experimentally.

It is shown that the iron losses and SLLs in IMs can be substantially higher than commonly considered, particularly in small standard-efficiency IMs. The exact amounts of the iron losses and SLLs largely depend on the operating torque, frequency, and flux. Without the appropriate IM model, it is impossible to evaluate them accurately in simulation studies, and the conventional IM model has proven inherently inadequate in this sense.

The proposed IM model accounts for only the fundamental harmonic-related iron losses and SLLs, so its validity is limited to a fundamental harmonic of the supply. Still, there is a great possibility of application of the proposed model in the development of advanced vector control schemes – including detuning analysis, loss optimization, or model-based speed and torque estimation.

Acknowledgements

This work has been fully supported by Croatian Science Foundation under the project (IP-2016-06-3319)

References

[1] P. L. Alger, *Induction Machines—Their Behavior and Uses*, 2nd ed. New York: Gordon and Breach, 1995.

[2] M. Bašić, D. Vukadinović, and M. Polić, "Stray load and iron losses in small induction machines under variable operating frequency and flux: a simple estimation method," *IEEE Trans. Energy Convers.*, Early Access Article (10.1109/TEC.2017.2759816).

[3] E. Levi, A. Lamine, and A. Cavagnino, "Impact of stray load losses on vector control accuracy in current-fed induction motor drives," *IEEE Trans. Energy Convers.,* vol. 1, no. 2, pp. 442-450, Jun. 2006.

[4] E. Levi, M. Sokola, A. Boglietti, and M. Pastorelli, "Iron loss in rotor-flux-oriented induction machines: identification, assessment of detuning, and compensation," *IEEE Trans. Power Electron.*, vol. 11, no. 5, pp. 698-709, Sep. 1996.

[5] M. Bašić and D. Vukadinović, "Vector control system of a self-excited induction generator including iron losses and magnetic saturation," *Control Engineering Practice*, vol. 21, no. 4, pp. 395-406, Apr. 2013.

[6] G. Bertotti, "Physical interpretation of eddy current losses in ferromagnetic materials. I. Theoretical considerations," *J. Appl. Phys.*, vol. 57, no. 6, pp. 2110-2117, Mar. 1985.

[7] S. S. L. Chang, "Physical concepts or stray load loss in induction machines," *Trans. Amer. Inst. Elect. Eng.*, vol. 73, no. 1, pp. 10-12, Jan. 1954.

[8] IEEE Standard Test Procedure for Polyphase Induction Motors and Generators (ANSI), IEEE Std 112-2004, 2004.

[9] Rotating Electrical Machines - Part 2-1: Standard Methods for Determining Losses and Efficiency from Tests (Excluding Machines for Traction Vehicles), IEC 60034-2-1:2014, 2014.

[10] A. Boglietti, R. Bojoi, A. Cavagnino, and S. Vaschetto, "Influence of the sinusoidal supply frequency on the induction motor stray load losses," in *Proc. IECON*, Montreal (QC), 2012, pp. 1847-1851.

[11] A. Boglietti, A. Cavagnino, L. Ferraris, and M. Lazzari, "Impact of the supply voltage on the stray-load losses in induction motors," *IEEE Trans. Ind. Appl.*, vol. 46, no. 4, pp. 1374-1380, July-Aug. 2010.

[12] A. Boglietti, A. Cavagnino, L. Ferraris, and M. Lazzari, "Induction motor equivalent circuit including the stray load losses in the machine power balance," *IEEE Trans. Energy Convers.*, vol. 23, no. 3, pp. 796-803, Sep. 2008.

[13] S. Shinnaka, "Proposition of new mathematical models with core loss factor for controlling AC motors," in *Proc. IECON*, Aachen, Germany, 1998, pp. 297-302.

[14] M. Bašić, D. Vukadinović, and G. Petrović, "Dynamic and pole-zero analysis of self-excited induction generator using a novel model with iron losses," *Int. J. Elect. Power Energy Syst.*, vol. 42, no. 1, pp. 105-

118, Nov. 2012.
[15] T. A. Nadjafabadi and F. R. Salmasi, "A flux observer with online estimation of core loss and rotor resistances for induction motors," *Int. Rev. Electr. Eng.*, vol. 4, no. 5, pp. 816-824, Oct. 2009.
[16] M. Hasegawa and S. Furutani, "Robust vector control of induction motors using full-order observer in consideration of core loss," *IEEE Trans. Ind. Electron.*, vol. 50, pp. 912-919, Oct. 2003.
[17] M. Bašić, D. Vukadinović, and I. Grgić, "Wind turbine-driven self-excited induction generator: a novel dynamic model including stray load and iron losses," *2nd Int. Multidisciplinary Conf. Computer and Energy Science*, Split, Croatia, July 12-14, 2017.
[18] G. C. D. Sousa and B. K. Bose, "Loss modelling of converter induction machine system for variable speed drive," in *IEEE Ind. Elec. Soc. Annu. Meeting IECON*, San Diego (CA), 1992, pp. 114-120.
[19] A. Vamvakari, A. Kandianis, A. Kladas, S. Manias, and J. Tegopoulos, "Analysis of supply voltage distortion effects on induction motor operation," *IEEE Trans. Energy Convers*., vol. 16, no. 3, 2001, pp. 209-213.
[20] Rotating Electrical Machines - Part 30-1: Efficiency Classes of Line Operated AC Motors, IEC 60034-30-1, 2014.
[21] A. Boglietti, A. Cavagnino, M. Lazzari, and M. Pastorelli, "Predicting iron losses in soft magnetic materials with arbitrary voltage supply: an engineering approach," *IEEE Trans. Magn.*, vol. 39, no. 2, pp. 981-989, Mar. 2003.
[22] M. Ranta, M. Hinkkanen, E. Dlala, A. K. Repo, and J. Luomi, "Inclusion of hysteresis and eddy current losses in dynamic induction machine models," in *Proc. IEMDC*, Miami (FL), 2009, pp. 1387-1392.
[23] D. M. Ionel, M. Popescu, S. J. Dellinger, T. J. E. Miller, R. J. Heideman, and M. I. McGilp, "On the variation with flux and frequency of the core loss coefficients in electrical machines," *IEEE Trans. Ind. Appl.*, vol. 42, no. 3, pp. 658-667, May-June 2006.
[24] D. M. Ionel, M. Popescu, M. I. McGilp, T. J. E. Miller, S. J. Dellinger, and R. J. Heideman, "Computation of core losses in electrical machines using improved models for laminated steel," *IEEE Trans. Ind. Appl.*, vol. 43, no. 6, pp. 1554-1564, Nov.-Dec. 2007.
[25] M. Popescu, D. M. Ionel, A. Boglietti, A. Cavagnino, C. Cossar, and M. I. McGilp, "A general model for estimating the laminated steel losses under PWM voltage supply," *IEEE Trans. Ind. Appl.*, vol. 46, no. 4, pp. 1389-1396, July-Aug. 2010.
[26] A. Boglietti, A. Cavagnino, D. M. Ionel, M. Popescu, D. A. Staton, and S. Vaschetto, "A general model to predict the iron losses in PWM inverter-fed induction motors," *IEEE Trans. Ind. Appl.*, vol. 46, no. 5, pp. 1882-1890, Sept.-Oct. 2010.

Mateo Bašić He received the B.S. degree and the Ph.D. degree in electrical engineering from the University of Split, Croatia, in 2006 and 2013, respectively. Since 2008, he has been with the University of Split, Faculty of Electrical Engineering, Mechanical Engineering and Naval Architecture, where he is currently an Assistant Professor. His research interests include modelling and control of electrical machines, power electronics, and artificial intelligence.

Dinko Vukadinović He received the B.S. degree from the University of Split, the M.S. degree from the University of Zagreb and the Ph.D. degree from the University of Split, Croatia, in 1997, 2002, and 2005, respectively, in electrical engineering. In 1998, he joined the University of Split, Faculty of Electrical Engineering, Mechanical Engineering and Naval Architecture, where he is currently a Full Professor and the Chair of Power Electronics and Control. His research interests include automation in electric power engineering, power electronics, electrical machines, and artificial intelligence.